Investigation of axially compressed frusta as impact energy absorbers

A. A. N. Aljawi and A. A. Alghamdi
Department of Mechanical Engineering, King Abdulaziz University, P.O. Box 9027, Jeddah 21413, Saudi Arabia
E-mail: aaljawi@hotmail.com & ajinaidi@kaau.edu.sa

Abstract

This paper reports, both experimentally and analytically, two new modes of plastic deformations of frusta when used as collapsible energy absorbers.

Deformable energy absorbers are briefly introduced, and their relevance in crash protection systems is stressed. A general review of literature is presented on energy absorption by metallic absorber of various cross sections with special attention to frusta. Experimental results for the two deformation modes of capped spun aluminum frusta under quasi-static testing condition are given. An Explicit version of ABAQUS 5.7-3 FE code is used for computing and describing the deformation modes of the frusta. Good agreement is obtained between the experimental results and the FE predictions.

1 Introduction

Energy absorbers are systems that convert kinetic energy into other forms of energy, such as pressure energy in compressible fluids, elastic strain energy in solids, and plastic deformation energy in deformable solids. The converted energy may be reversible, as in pressure energy in compressible fluids, and elastic strain energy in solids, or irreversible, as in plastic deformation. The process of conversion for plastic deformation depends, among other factors, on the magnitude and method of application of loads, transmission rates, deformation displacement patterns and material properties [1].

The predominant domain of applications of collapsible energy absorbers is that of crash protection. Such systems are installed in high-risk environments with potential injury to humans or damage to property. The aim is to minimize the risk of injury or damage by controlling the deceleration pulse during impact. This is achieved by extending the period of dissipation of the kinetic energy of the system over a finite period of time. Cushioning devices on vehicle bumpers, crash retards in emergency systems of lifts and crash barriers used as roadblocks are everyday examples.

Familiar deformable energy absorber units include cylindrical shells [2], wood-filled tubes [3], foam-filled columns [4], sand-filled tubes [5], steel barrels [6], PVC shells [7], tube inversions [8] and tubular elements [5] and a variety of shapes and arrangements. The active absorbing element of an energy absorption system can assume several common shapes such as circular tubes [9], square tubes [10], multicorner metal columns [11], frusta [12], strips [13] and rods [14].

Developments of mechanical devices that help dissipate kinetic energy at predetermined rates have been receiving substantial attention for several decades [15]. When designing a collapsible energy absorbing (dissipating) device, the prime aim is to absorb the majority of the kinetic energy of impact within the device itself in an irreversible manner. The absorbing system must exhibit force-deflection characteristics, which result in decelerations that are within allowable limits. These limits may be dictated either by human tolerance levels or by the maximum force the structures themselves can withstand [13].

Axisymmetrical and circular shapes provide perhaps the widest range of all choices for use as absorbing elements because of their favorable plastic behavior under axial forces, as well as their common occurrence as structural elements.

In this paper the selected absorber has a truncated capped frustum shape. Frusta are employed over a wide range of applications, especially in the domains of aerospace and armaments. Common examples occur in the nose cones of missiles and aircraft. The following section highlights only the axial crushing of this tubular absorber, since the proposed deformation modes are due to axial loads. Section 3 gives the finite element modeling whereas the experimental setups are given in Section 4. Results are discussed in Section 5 and some observations and remarks in Section 6 conclude the paper.

2 Axial Loading of Tubular Components

The study of deformation of tubular energy absorbers in general falls into two main categories; lateral, and axial loading. Investigations often lead to accounting for geometrical changes, interactions between modes of collapse, as well as strain hardening and strain rate effects.

Johnson and Reid [13] identified the dominant modes of deformation in simple structural elements in the form of circular and hexagonal cross-section tubes when these elements were subjected to various forms of quasi-static loading. They described the load-deformation characteristics of a number of these elements.

Thin-walled absorbers having symmetrical cross sections may collapse in concertina or diamond mode when subjected to axial loads. The collapsing of such components by splitting or by inversion is also conceivable [10].

The behavior of thin tubes (diameter D/ thickness t> 50), with circular and square cross sections, when subjected to axial loads, has been of particular interest since the pioneering works of Alexander [2] and Pugsley and Macaulay [16]. In fact circular tubes under axial compression are reported to be the most prevalent components in energy absorber systems. This is because the circular tube provides a reasonably constant operating force. Furthermore, circular tubes have comparatively high energy absorbing capacities, and stroke length per unit mass. In comparing lateral with axial compression, the axial buckling mode has a specific energy absorbing capacity, which is approximately ten times that of the same tube when compressed laterally between flat plates [6]. Moreover, practically all wall material in a tube can be made to participate in the absorption of energy by plastic work in axial loading.

Experimental observations show that thick-walled cylinders buckle in concertina (axisymmetric) mode of deformation, whereas thin-walled cylinders buckle in diamond (non-axisymmetric) mode of deformation. For large values of D/t diamond-fold mode of deformation tends to occur, and the number of lobes increases with D/t ratio [9].

2.1 Thin-Walled Frusta

Frusta are truncated circular cones, see Figs. 1&2. Literature on the utilization of frusta for dissipation of energy is meager. Postlethwaite and Mills [12] first studied the frustum in this context in 1970. In their study of axial crushing of conical shells they used Alexander's extensible collapse analysis [2] to predict the mean crushing force for the concertina mode of deformation for frusta made of mild steel.

Mamalis et al. [17] investigated experimentally the crumbling of aluminum frusta when subjected to axial compression load under quasi-static conditions. They proposed empirical relationships for both the concertina and the diamond modes of deformation. Mamalis et al. [18] extended their experimental study to include mild steel at elevated strain rates. They concluded that the deformation modes of frusta could be classified as a) concertina, b) concertina-diamond, and c) diamond. Mamalis and associates [19] refined the work of Postlethwaite and Mills [12] in using the extensible collapse analysis for predicting the mean crushing load, and fair agreement with the experimental results were reported. In another paper Mamalis and his co-workers [7] investigated the crumbling of PVC frusta. In another paper, Mamalis and his group [20] modeled the progressive extensible collapse of frusta and gave a theoretical model that depicts the changes in peaks and troughs of the experimental load-displacement curves. The comparison with the experimental results gave a fair degree of accuracy.

The above studies deal with axial crushing (or crumbling) of frusta between two parallel plates. However, two innovative modes of axial deformation are

presented in this paper. These modes are inward (free or direct) inversion and outward (or indirect) flattening.

In what follows, results of experimental work as well as finite element modeling conducted on the inward inversions and outward flattening of capped spun aluminum frusta are presented.

3 Finite Element Modeling

The finite element method (FEM) has been used extensively to simulate many applications in structural dynamics [9,21-23]. In the present study, ABAQUS Explicit FEM code (version 5.7-3) is employed to investigate the modes of deformation of frusta under quasi-static loading. Figs. 3&4 show the finite element models used in this study for inward inversion and outward flattening, respectively. An axisymmetric four-nodded element, CAX4R, is used for modeling the frustum shown in Figs. 3 & 4. About 300 elements are used for the model. Material properties of the model in the elastic range were taken as modulus of elasticity, E=70 GPa, Poisson's ratio, ν=0.3, and density ρ=2800 Kg/m^3, and fully plastic in the plastic range with yield strength S_y=125 MPa. In both cases of inversion and flattening, all nodes at the centerline of symmetry were selected to move only in the vertical direction.

Both upper and lower surface were set in contact with rigid body surfaces. These rigid surfaces were modeled using two nodal axisymmetric rigid elements, RAX2. A coefficient of friction of μ=0.15 was incorporated between the contact surfaces. A reference node was introduced at the top end surface of the model. This node was set to move at a velocity of 0.01m/s representing quasi-static case.

In inward inversion, the upper small capped end of the frustum was in contact with a rigid body moving at a constant velocity. The lower end was restrained from moving in vertical and horizontal directions as shown in Fig. 3. In outward flattening, the upper small capped end was in contact with the rigid body. However, the size of the rigid body was larger than the large diameter of the frustum. The lower end of the frustum was constrained to move in the vertical direction only, see Fig. 4.

4 Experimental

Preliminary trials of inward inversion were conduct on aluminum frusta that were produced by spinning. Consequently all frusta for the experimental program were manually spun from blanks of commercial aluminum sheets 0.5, 1.0,1.5, and 2.0 mm in thickness. Three different mandrels featuring angles (α) of 30°, 45°, and 60°, were manufactured for the spinning process. As they were not subjected to subsequent heat treatment, the frusta produced by cold spinning featured locked-in residual stresses. Moreover, axial variations were noticeable in the thickness of the shell of the frusta.

A large number of frusta, featuring different thicknesses and apex angles were subjected to various loading conditions. The program involved the use of

twelve different sizes of aluminum frusta (3 different apex angles and 4 different thicknesses) for inward inversion and outward flattening. Additional tests were conducted to investigate the effect of impact speed on inversion and flattening.

Tests were conducted by the use of a 50-ton Instron Universal Testing machine (UTM) as well as a falling weight hammer (FWH) of 10 m/s striking speed. Two special jigs, one for inward inversion, and the other for outward flattening were manufactured and utilized. The inward inversion jig consisted of an inversion rod and a base cylinder, as shown in Fig. 1. The upper jaw of the UTM clamped the rod, and the base rested on the lower jaw. The setup for outward flattening comprised essentially two parallel plates. The upper jaw of the UTM gripped the upper plate, and the lower plate rested on the lower jaw, see Fig. 2. Both jigs were utilized also with the FWH, in which case the inversion rod and the upper plate were simply placed on the specimen.

5 Results and Discussion

In this section details of the experimental load-displacement curves and finite element results for both inward inversion and outward flattening are presented in detail for quasi-static loading.

5.1 Inward inversion

Fig. 5 shows experimental and finite element (FE) load-displacement curves for spun aluminum frusta in inward inversion at a cross-head speed of 10mm/min. The specimen has an angle α=60°, large diameter D=73 mm, small diameter d=22.5 mm, thickness t=1.25mm, and mass m=25.72grams. It can be observed that good agreement is obtained between the experimental results and FE predictions. The FE details of the inward inversion process can be seen in Fig. 6 that gives the stages of the inward inversion. Fig. 7 is a photograph showing the specimen during inward inversion.

It can be observed from Fig. 5 that the frustum passes through a number of stages. The load rises quasi-linearly from the origin to point (a). The force at point (a) represents the load of instability. Up to this point the deformation is recoverable, i.e., elastic and beyond which plastic behavior sets in. The zone between (a) and (b) is a zone of incubation, within which the cap of the frustum is deformed in such a manner as to facilitate the inversion type of deformation. Point (b) signals completion of the development of the inversion zone. Inversion then proceeds towards the larger (lower) end of the frustum, until point (c) is reached. The increase in the inversion force from (b) to (c) is attributed to the progressive increase in the volume of the deformation zone with the increasing D/t ratio.

Point (c) in Fig. 5 signals the termination of the inversion zone, the bending front having reached the vicinity of the free large end of the frustum. From point (c) to (d) inversion mode changes into flattening mode and the undeformed part of the frustum has the shape of Belleville spring. The free end of the frustum is

flattened parallel to the shoulder of the jig base. The energy absorbed by the frustum through this inward inversion is 9.73 J/gm.

In order to assess the effect of speed on the process of inversion and flattening, identical frusta were tested at cross-head speeds of 2, 20 and 200 mm/min. Additional tests were conducted on the FWH facility for both inward inversion and outward flattening. As all specimens in these tests behaved as in quasi-static tests, it was concluded that the processes of inversion and flattening are not affected by strain rate for low impact velocities.

The possibility of re-using the inverted frusta was investigated. Several tests were conducted for inversion and then re-inversion of inverted frusta. Although not shown, results from one such experiment show that it is possible to invert, re-invert and then again invert an aluminum frustum. All specimens failed, however, during the fourth inversion.

5.2 Outward Flattening

A number of tests were undertaken for the outward flattening of frusta between two parallel plates. The experimental load-displacement curve and FE predictions for a typical test are displayed in Fig. 8. The specimen used has D=75 mm, d=23 mm, t=1.9 mm, α=45°, and mass=27.8 grams. The stages of outward flattening process modeled by FE can be seen in Fig. 9. A photograph showing the experiment of outward flattening is shown in Fig. 10.

As in the case of tube inversion [8], elastic behavior is observed up to point (a) in Fig. 8. Point (a) is the point of plastic instability, at which the rim of the lower end deforms into the shape of a funnel. The decrease in the flattening force between points (a) and (b) signifies the development of the free readjusting of the lip at this end. The force increases again after point (b), as material is being pushed radially outward while the diameter of the deformation zone decreases. At point (c) the zone of outward flattening is fully developed, and the lip of the inverted rim curls upward from the lower plate. The section of the curve from (c) to (d) depicts the progressive first outward inversion at the lower plate. The sharp rise represented by the (d)-(e) sector develops when the rising lip of the inverted rim meets the upper plate, which forces it to bend (re-invert) downwards, in the direction opposite to the direction of the first outward inversion. This is followed by the development of a second inversion zone (e to f), where residual stresses from the first inversion are thought to be the cause of the lowering of the load in this sector. The frustum is being crushed flat at point (g). The energy absorbed by the frustum through outward flattening is 9.89 J/gram, which is slightly larger than the value for inward inversion.

6 Conclusions

To compare the inversion and flattening characteristics of frusta with those of thin tubes, it must be pointed out that tube inversion cannot be executed unaided,

since a minimum of one die is required for the process. A second and important drawback of tube inversion is that there is a maximum tube height that is determined by the mean diameter and the wall thickness, which if exceeded, failure occurs due to elastic buckling and not due to inversion. Furthermore, tube inversion is limited to about half the original tube height unless special, costly arrangements are incorporated. None of these shortcomings are encountered during the inversion and flattening of frusta.

The mode of deformation was always consistent with the type of jig in use. In fact it was found that an absorber in the inversion mode might be inverted several times, indicating that it is possible re-use the same absorber. Since all specimens in the impact tests behaved as in the quasi-static tests, it is concluded that within the experimental range of impact speeds (0-7m/s), the processes of inversion and flattening are not affected by the speed of deformation.

It is concluded from a comparison of the results of tests involving inward inversion with those of outward flattening that the overall amount of energy absorbed in inward inversion is the same as that of outward flattening

Finally, good agreement was achieved between the experimental results and the predictions by the FE model at the condition investigated.

8 Acknowledgement

The authors would like to thank King Abdulaziz City for Science and Technology for their support of this research through grant number LG-2-74, 1998. Thanks to Professor Mehmet Akyurt for his valuable comments and help in preparing this manuscript.

9 References

1. Reid, S.R., Drew, S.L.K. & Carney, J.E., Energy absorbing capacities of braced metal tubes, *Int. J. Mech. Sci.*, **25**, pp. 649-667, 1983.
2. Alexander, J.M., An approximate analysis of the collapse of thin cylindrical shells under axial loading, *Quart. J. Mech. Appl. Math.*, **13**, pp. 10-15, 1960.
3. Reddy T.Y. & Al-Hassani, S.T.S., Axial crushing of wood-filled square metal tubes, *Int. J. Mech. Sci.*, **35**, pp. 231-246, 1993.
4. Abramowicz, W. & Wierzbicki, T., Axial crushing of foam-filled columns, *Int. J. Mech. Sci.*, **30**, pp. 263-271, 1988.
5. Reid, S.R., Metal tubes as impact energy absorbers, *Metal Forming and Impact Mechanics*, ed. S. R. Reid, Pergamon, New York, pp. 249-269, 1985.
6. Carney III, J.F. & Pothen, S., Energy dissipation in braced cylindrical solids, *Int. J. Mech. Sci.*, **30**, pp. 203-216, 1988.
7. Mamalis, A.G., Manolakos, D.E., Viegelahn, G.L., Vaxevanidis, N.M. & Johnson, W., On the inextensional axial collapse of thin PVC conical shells, *Int. J. Mech. Sci.*, **28**, pp. 323-335, 1986.
8. Al-Hassani, S.T.S., Johnson, W. & Lowe, W.T., Characteristics of inversion tubes under axial loading, *J. Mech. Eng. Sci.*, **14**, pp. 370-381, 1972.

9. Reid, S.R., Plastic deformation mechanisms in axially compressed metal tubes used as impact energy absorber, *Int. J. Mech. Sci.*, **35**, pp. 1035-1052, 1993.
10. Lu, G., Ong, L.S., Wang, B. and Ng, H.W., An experimental study on tearing energy in splitting square metal tubes, *Int. J. Mech. Sci.*, **36**, pp. 1087-1097, 1994.
11. Abramowicz, W. & Wierzbicki, T., Axial crushing of multicorner sheet metal columns, *J. Appl. Mech.*, **56**, pp. 113-120, 1989.
12. Postlethwaite, H.E. & Mills, B., Use of collapsible structural elements as impact isolators with special reference to automotive applications, *J. Strain Anal.*, **5**, pp. 58-73, 1970.
13. Johnson, W. & Reid, S. R., Metallic energy dissipating systems, *Appl. Mech. Rev.*, **31**, pp. 277-288, 1978.
14. Alghamdi, A.A. & Aljawi, A.A.N., Cubic steel rod cells as energy absorbers, Proceedings of the 7th International Conference in Mechanical Design and Production, Cairo, Egypt, February 15-17, 2000, submitted.
15. Jones, N., Recent studies in the dynamic plastic behavior of structures, *Appl. Mech. Rev.*, **42**, pp. 95-115, 1989.
16. Pugsley, A.G & Macaulay, M., The large-scale crumpling of thin cylindrical columns, *Quart. J. Mechs. App. Math.*, **13**, pp. 1-9, 1960.
17. Mamalis, A.G. & Johnson, W., The quasi-static crumpling of thin-walled circular cylinders and frusta under axial compression, *Int. J. Mech. Sci.*, **25**, pp. 713-732, 1983.
18. Mamalis, A.G., Johnson, W. & Viegelahn, G.L., The crumbling of steel thin-walled tubes and frusta under axial compression at elevated strain-rate: some experimental results, *Int. J. Mech. Sci.*, **26**, pp. 537-547, 1984.
19. Mamalis, A.G., Manolakos, D.E., Saigal, S., Viegelahn, G. & Johnson, W., Extensible plastic collapse of thin-wall frusta as energy absorbers, *Int. J. Mech. Sci.*, **28**, pp. 219-229, 1986.
20. Mamalis, A.G., Manolakos, D.E., Viegelahn, G.L. & Johnson, W., The modeling of the progressive extensible plastic collapse of thin-wall shells, *Int. J. Mech. Sci.*, **30**, pp. 249-261, 1988.
21. Bammann, D. J., Chjiesa, M. L., Horstemeeyer, M. F. & Weigaten, L. T., Failure in ductile materials using finite element methods, *Structural Crashworthiness and Failure*, ed. N. Jones & T. Wierzbick, Elsevier, London, pp. 1-54,1993.
22. Kormi, K., Shaghouei, E. & Duddell, D.A., Finite element examination of dynamic response of clamped beam grillages impacted transversely at their center by a rigid mass, *Int. J. Impact Eng.*, **15**, pp. 687-697, 1994.
23. HKS, Inc, ABAQUS/Explicit User's Manual, Theory and examples manuals and post manual, Version 5.7, Explicit, 1997.

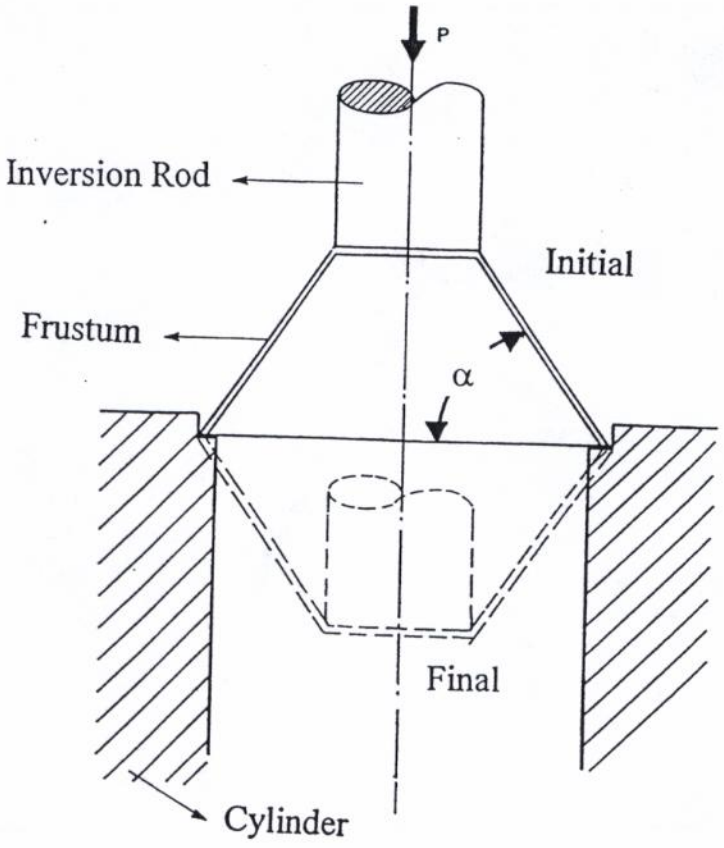

Figure 1. Inward (direct) inversion of frusta.

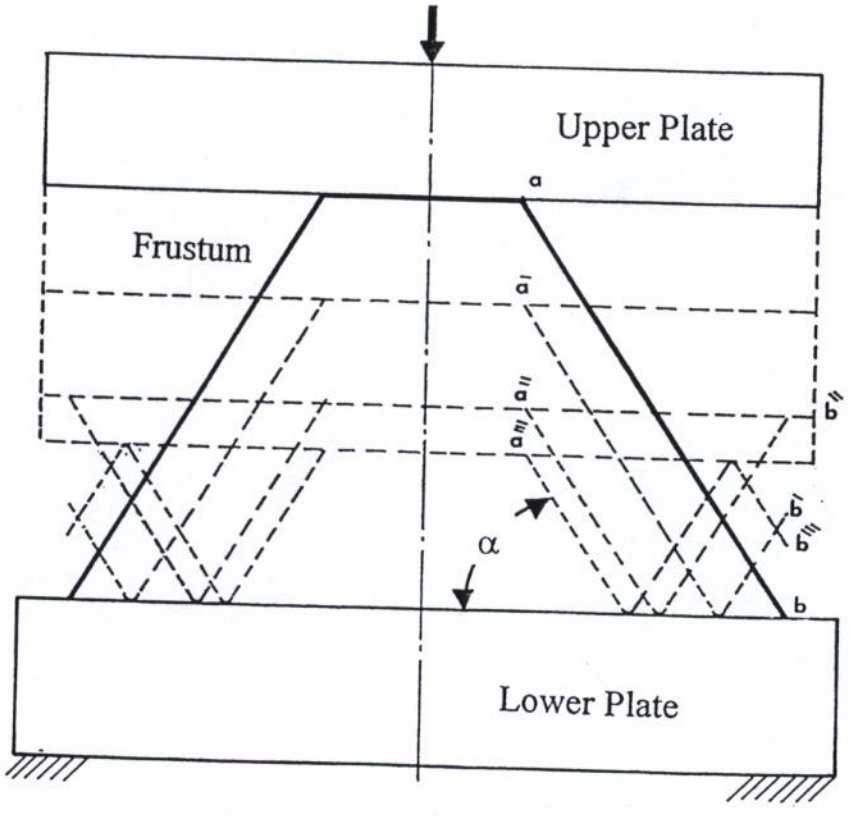

Figure 2. Outward (indirect) flattening of frusta.

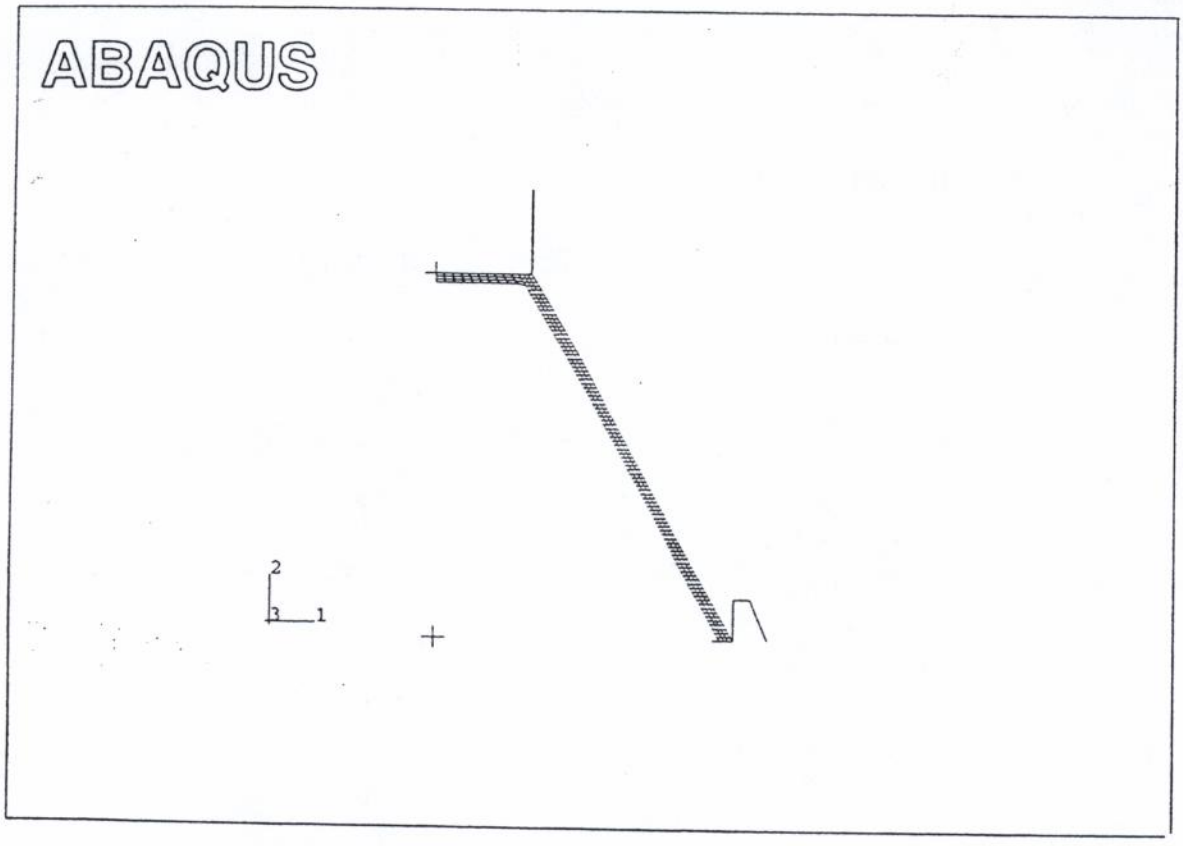

Figure 3. FE model for direct inversion.

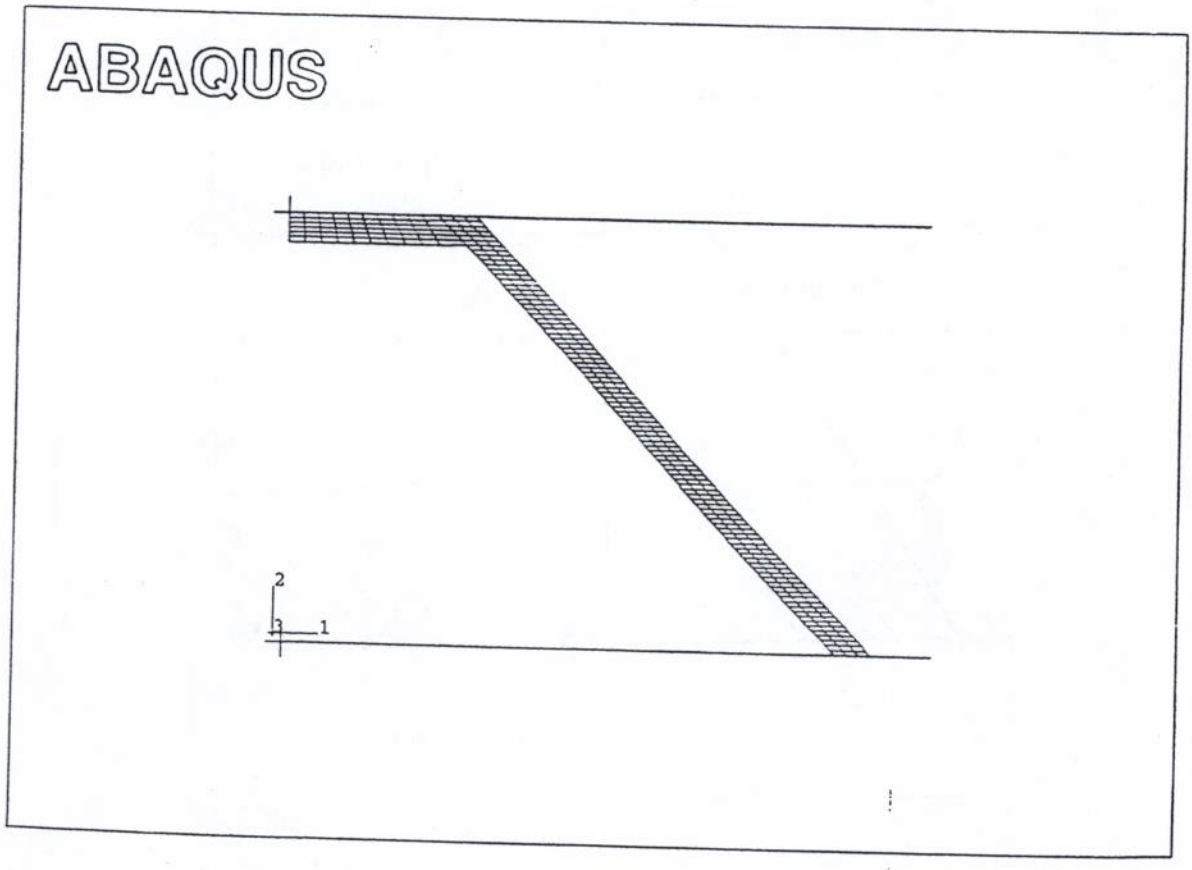

Figure 4. FE model for flattening of frusta.

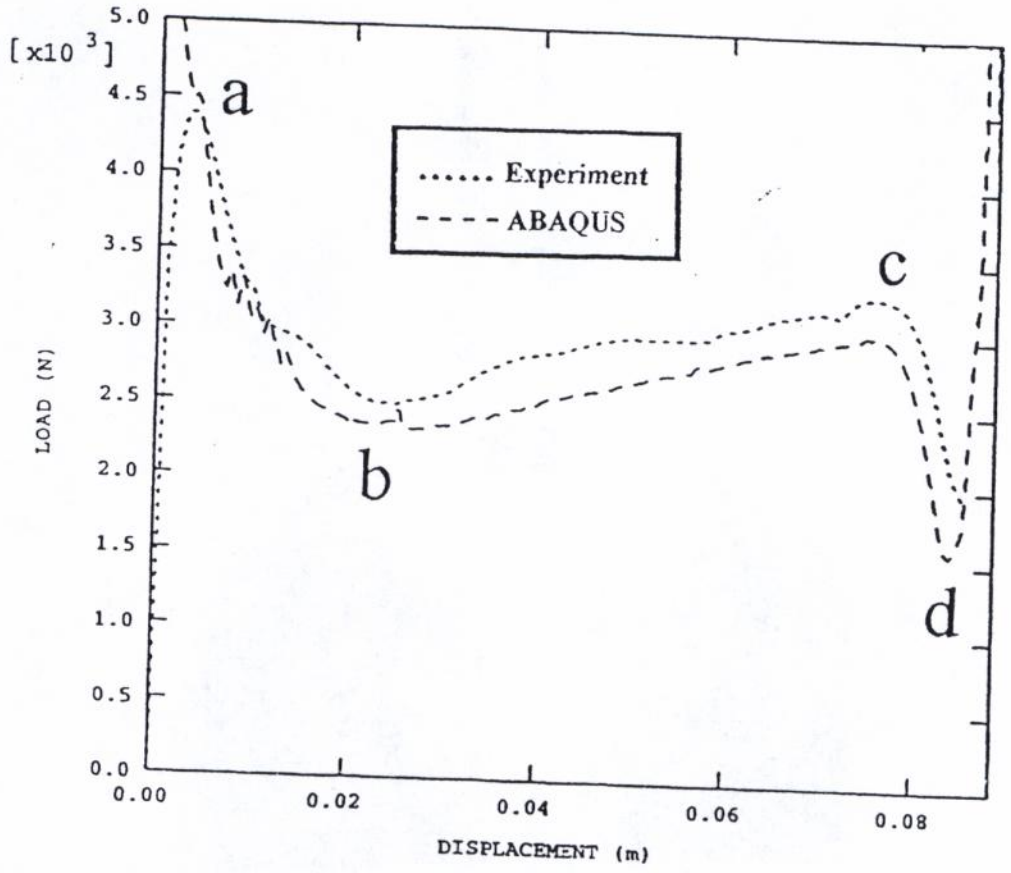

Figure 5. Experimental FE load-displacement curves for quasi-static inward inversion of aluminum frustum.

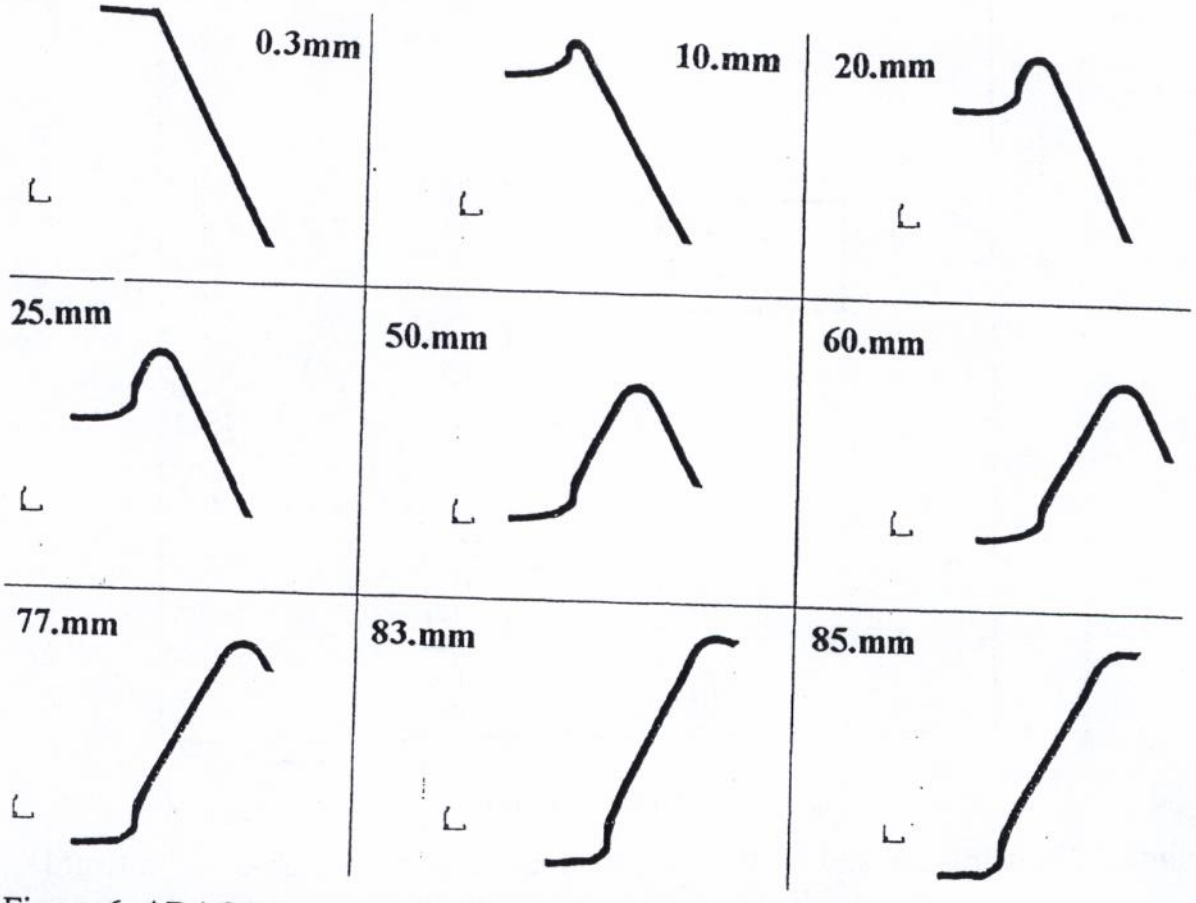

Figure 6. ABAQUS deformed plots for inward inversion of aluminum frustum.

Figure 7. Photograph showing the direct inversion of frusta.

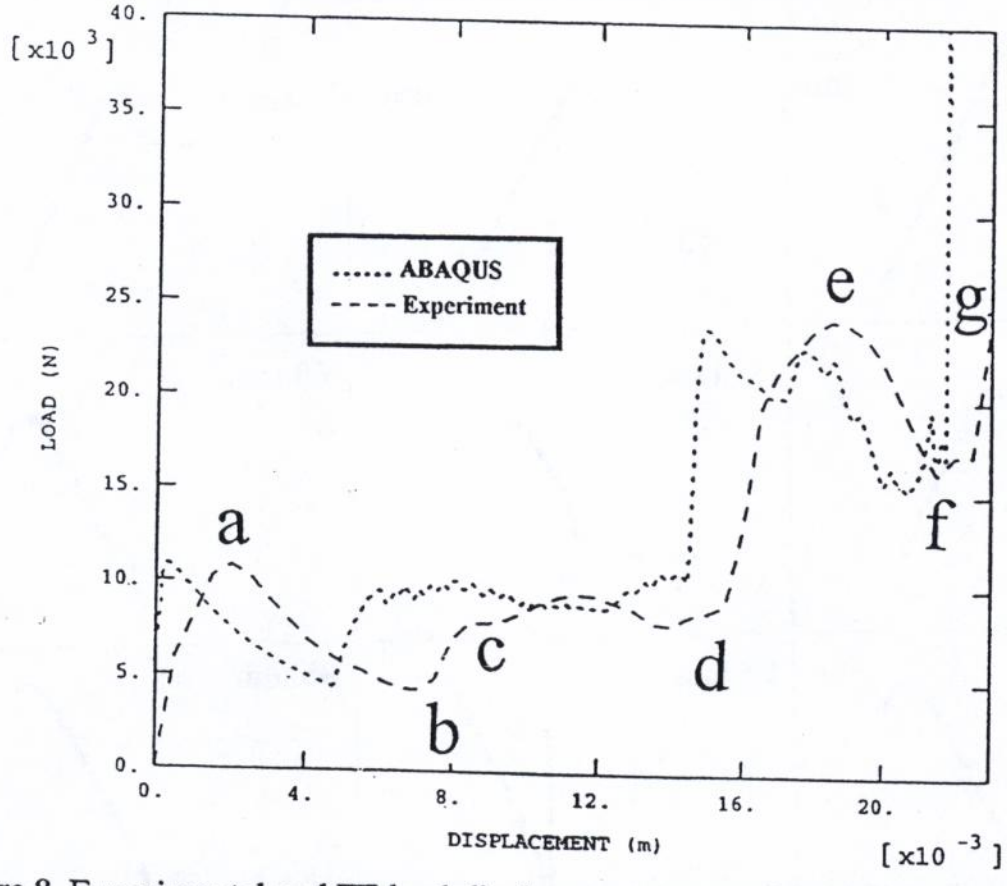

Figure 8. Experimental and FE load-displacement curves for quasi-static outward flattening of aluminum frustum.

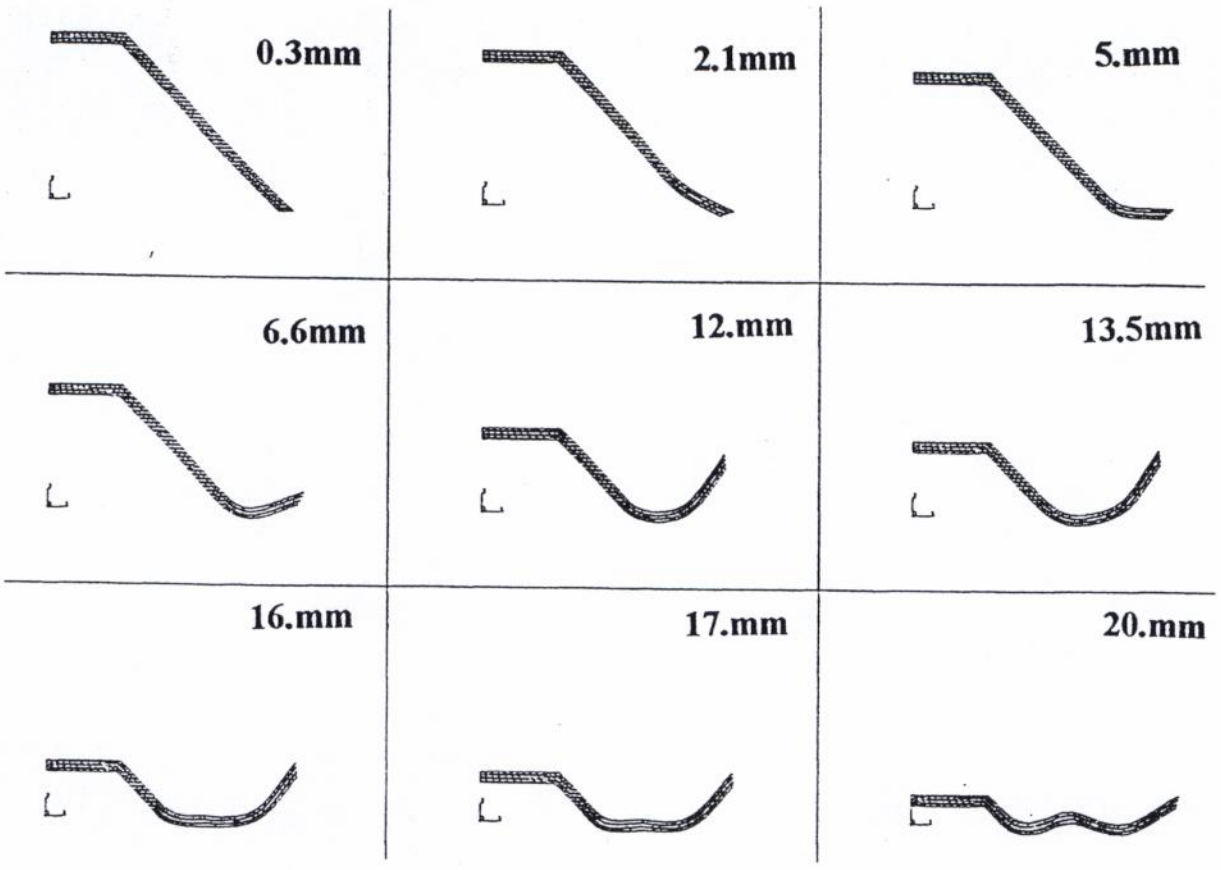

Figure 9. ABAQUS deformed plots for static outward flattening of aluminum frustum.

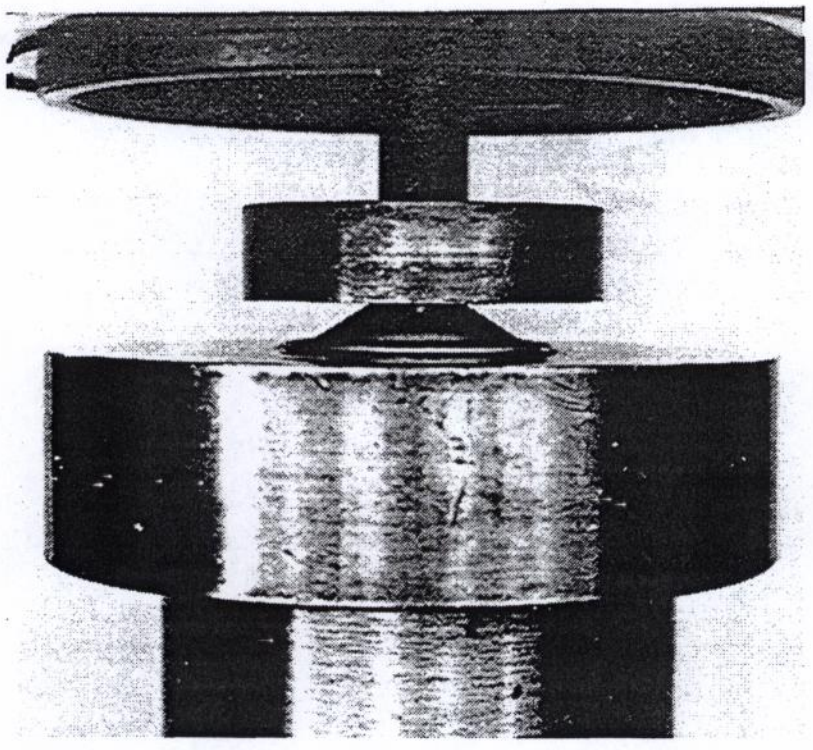

Figure 10. Photograph showing the outward flattening of frusta.